nature communications

Article

https://doi.org/10.1038/s41467-025-58864-6

Room-temperature phosphorescence and anomalous piezochromism in molecular crystals enabled by iodine atomic orbital sharing

Received: 22 May 2024

Accepted: 31 March 2025

Published online: 14 April 2025

Check for updates

Tongge Xu, Chunguang Zhai ✉, Ziyao Liu, Xiaoying Yang, Shuhe Hu, Yuchen Shang, Lei Yue, Jiajun Dong, Ran Liu, Quanjun Li, Mingguang Yao ✉ & Bingbing Liu

Controlling room-temperature phosphorescence (RTP) in organic materials through external stimuli is crucial for elucidating RTP mechanisms and engineering stimuli-responsive materials for various applications. However, compared to fluorescent materials, regulating RTP presents greater challenges due to its intricate photophysical processes, particularly in the quest for RTP materials with desirable stimulus-responsive properties. Here we show that when the interactions of iodine with neighboring molecules in 1,4-diiodotetrafluorobenzene (1,4-DITFB) crystals are tuned by pressure, exotic emission behaviors emerge. These emissions exhibit anomalous blue-shifted characteristics and enhanced intensities upon compression, accompanied by prolonged lifetimes. Notably, such piezochromic luminescence responses are impeded through a co-crystallization strategy that hinders iodine-iodine interactions. We further reveal that the observed anomalous emissions related to the unique state of iodine by providing additional orbitals shared with surrounding molecules. Our findings not only open pathways for designing tailored stimuli-responsive luminescent materials but also offer valuable insights into the underlying mechanisms governing organic RTP emitters.

Organic room-temperature phosphorescence (RTP) materials have garnered significant research attention owing to their inherent advantages compared to fluorescent materials, such as long lifetimes, large Stokes shifts, rich excited state properties[1–5]. These significant advantages make organic RTP materials exhibit great potential in the design of stimuli-responsive luminescent materials for diverse applications, such as smart sensors, bioimaging, and optoelectronic devices[6–10]. For this purpose, investigating the responses of RTP materials to external stimuli has emerged as a particularly attractive research area. Hydrostatic compression, a prevalent stimulus, offers advantages in emission tuning and establishing structure-property relationships of materials in a more controllable manner, thereby serving as a vital platform for property modulation and mechanism comprehension[11,12]. This has prompted numerous studies on piezochromic luminescent materials in the past decade[13–15]. However, most of the organic luminescent materials reported so far exhibit red-shifted and quenched emission upon compression[16,17], which is due to the compression-induced unavoidable energy bandgap decrease as well as increased non-radiative de-excitation and vibrational relaxation[18,19]. It is thus difficult to design piezochromic luminescent materials with anomalous blue-shifted and enhanced emission upon compression, with only a few instances of success observed in

State Key Laboratory of High Pressure and Superhard Materials, College of Physics, Jilin University, Changchun, China. ✉e-mail: zhaicg@jlu.edu.cn; yaomg@jlu.edu.cn

fluorescent organic materials[20–23]. This challenge is further compounded in RTP organic materials due to the complex behaviors of triplet excitons, spin-forbidden transition, intersystem crossing, etc.[24,25]. Therefore, investigating RTP materials with desirable stimulus-responsive properties and elucidating structure-property correlations is pivotal for advancing both the fundamental understanding of phosphorescence mechanisms and the development of potential applications.

From the electronic structure point of view, RTP is strongly affected by the coupling of excited singlet and triplet states of electrons[26–28]. Therefore, modulating RTP emission is not only required to regulate the optical bandgap of singlet and triplet states, respectively, but also the electron transition behaviors from singlet to triplet states. In addition, the heavy atom effect of halogen plays a crucial role in enhancing spin-orbit coupling (SOC) and accelerating intersystem crossing (ISC)[28–31], which enables excitations with different orbital momenta for singlet and triplet states, and thus facilitates the RTP emission. Recent studies have shown that high pressure can induce significant enhancement of atomic/molecular interactions, which may extrude electrons from atoms into the voids or vacancies of crystals, forming so-called interstitial quasi-atoms (ISQs)[32]. These ISQs can form covalent or metallic bonds with neighboring atoms, resulting in quantized orbitals of interstitial space and significantly changing electronic structures and properties of materials[33]. Additionally, our recent investigations have revealed that controlling the nearest neighboring molecular interactions could significantly modulate electronic structures in molecular crystals and tune their luminescent properties[21,22,34]. This approach holds promise as a potential avenue for designing exceptional stimuli-responsive properties.

In this work, we realize anomalous pressure-responsive RTP in 1,4-diiodotetrafluorobenzene (1,4-DITFB) molecular crystals by enhancing the shared orbitals of iodine with the surrounding atoms/molecules and SOC. We discover that atomic orbitals of iodine become shareable with neighboring molecules in 1,4-DITFB crystals upon compression, triggering RTP emission from the initial non-RTP emission state. Such states of iodine become more significant and cause unexpected and continuous blue-shifted and enhanced RTP emission upon further compression, accompanied by prolonged lifetimes, which have never been realized before. Further comparison experiments show that the anomalous blue-shifted RTP emission disappears when the halogen-halogen interactions in 1,4-DITFB crystals are hindered by inserting other molecules.

Results

Photophysical properties of 1,4-DITFB crystals upon compression

The X-ray diffraction (XRD) pattern (Supplementary Fig. 1) shows that 1,4-DITFB molecular crystals exhibit a monoclinic structure characterized by a "herringbone" motif[35] primarily assembled through halogen bonding at ambient pressure. The structural sketch map is shown in Supplementary Fig. 2. The crystals are almost non-emissive at ambient pressure but display remarkable photoluminescence (PL) emission under high-pressure stimulation. The high-pressure PL spectra of 1,4-DITFB crystals recorded by 355 nm excitation are shown in Fig. 1a–d, which exhibit an abnormal PL behavior as pressure increases. The weak emission center gradually shifts from near 480 nm to a new emission center at 652 nm below 1 GPa (Fig. 1d), while this PL peak exhibits an abnormal blueshift to 582 nm and a significant enhancement in emission intensity as pressure increases to 7.50 GPa (Fig. 1a, b, e). Above 7.50 GPa, the emission intensity gradually decreases, but the emission bands remain blue-shifted to 561 nm with increasing pressure (Fig. 1c, e). The CIE chromaticity diagram (Fig. 1f) and PL photographs (Fig. 1g) of 1,4-DITFB clearly show a color change from red to yellow-green as pressure increases. At pressures exceeding 14.61 GPa, the 1,4-DITFB crystal turns red-shifted and quenched emission (Fig. 1d).

In situ time-resolved photoluminescence (TRPL) measurements were carried out to analyze the components of PL and the dynamics of excited states. As shown in Fig. 2a, the PL decay signal exhibits nanosecond lifetimes below 0.91 GPa ($\tau = 0.26$ ns under ambient conditions and $\tau = 0.21$ ns at 0.91 GPa), indicating very weak fluorescence without phosphorescence at low pressures (Fig. 1d). Low-temperature PL and TRPL measurements suggest that no phosphorescent emission can be detected in 1,4-DITFB crystals and the 1,4-DITFB dilute solution has no any emission at ambient pressure due to the absence of the triplet emission property, rather than due to vibrational quenching or triplet-triplet annihilation (TTA) (Supplementary Fig. 3). Nevertheless, a long-lived microsecond lifetime component emerges and progressively increases upon further compression (Fig. 2b), reaching a maximum average lifetime of $\tau = 3.39$ μs at ~6.94 GPa (Fig. 2c, d), concomitant with an increase in emission intensity as pressure increases. This new emission should be phosphorescence and gradually become dominant upon compression. Furthermore, we carried out in situ ultraviolet-visible (UV-Vis) absorption spectra on 1,4-DITFB to investigate the changes in its band gap under pressure. From the recorded UV-Vis absorption spectra (Fig. 2e and Supplementary Fig. 4) we can see that the band gap of 1,4-DITFB is 3.78 eV at 0.22 GPa and exhibits an obvious redshift upon compression (Fig. 2f). Note that the redshift of the absorption edge and the blueshift of the PL peak indicate that a gradual decrease in the singlet and triplet splitting energy (ΔE_{ST}). Following the energy gap law, the reduction of ΔE_{ST} favors ISC between singlet and triplet states, which contributes to phosphorescence emission. Such a strategy of minimizing ΔE_{ST} has also been previously reported to design more efficient and persistent pure organic RTP emitters[36,37]. It is noteworthy that in pure organic molecular systems, emission under pressure typically undergoes a redshift, with only a very few cases exhibiting a blueshift, which is always accompanied by a blueshift in absorption[20,21], while the lifetime of phosphorescence reported so far consistently decreases as pressure increases[38]. In contrast to the studied pure aromatic hydrocarbons with weak hydrogen bonding and π−π interactions, our 1,4-DITFB crystals display a distinctive pressure-induced blue-shifted RTP emission, which should be attributed to the incorporation of halogen atoms (I and F) that create significant intermolecular halogen-halogen interactions, thereby changing the electronic structure of the excited states[39].

High-pressure structural evolution of 1,4-DITFB crystals

High-pressure XRD experiments were carried out on 1,4-DITFB crystals to investigate their structural changes and explore the underlying mechanism for the anomalous RTP emission. As shown in Fig. 3a, b, no structural transition is observed in the crystal below 9.02 GPa, but above this threshold, the gradual weakening and broadening of diffraction peaks suggest progressive structural amorphization, which is responsible for the gradual weakening of RTP emission upon compression. Such amorphization could destroy the initial luminescence energy levels and cause strong emission-detrimental intermolecular interactions, leading to a rapid nonradiative decay of excitons[40,41]. Note that the *a*-, *b*-, and *c*-axes undergo distinct pressure evolutions upon compression (inset, Fig. 3b), with the *c*-axis being more compressible than the *a*- and *b*-axes below 7.95 GPa. Considering the molecular packing (Fig. 3c), such an obvious anisotropic compressibility of the lattice could facilitate the rapid approach of halogen atoms and thereby increase the halogen-halogen interactions (I···I, I···F, and F···F interactions). The Hirshfeld surface (HS) analysis[42] further demonstrates that high pressure significantly enhances intermolecular halogen-halogen interactions (Fig. 3d).

Intermolecular interactions of 1,4-DITFB crystals by IR and Raman spectroscopies

As there was no structural transition in the compressed crystal, we further performed in situ infrared (IR) and Raman spectroscopy measurements to investigate the intermolecular interactions in 1,4-DITFB crystals under pressure. As shown in Fig. 4a and Supplementary Fig. 5, most of the IR absorption peaks are normally blue-shifted upon compression, suggesting the enhancement of intermolecular interactions[43]. However, the IR peaks representing the combination band of ring vibrations and the B_{2u} mode of aryl sextant C–C stretch[44] (located near 1269 and 1355 cm^{-1}, respectively) exhibit a continuous redshift (Fig. 4b). Such behavior in molecular crystals usually indicates the inhibition of non-radiative energy dissipation, thereby favoring radiative energy enhancement within 1,4-DITFB molecules upon compression[45]. Our high-pressure Raman measurements show that the molecular vibrational peaks mostly exhibit a blueshift upon compression (Fig. 4c). Remarkably, the A_g vibrational mode of the C–I symmetric stretching located near 157 cm^{-1} undergoes triple splitting above 1.57 GPa (Fig. 4d, e), corresponding to the pressure at which the significant enhancement and blueshift of RTP occur. And most of the Raman modes in the low frequency region (below 157 cm^{-1}) progressively increase in intensity with increasing pressure, suggesting a substantial increase in molecular polarizability[46] within 1,4-DITFB crystals. These results indicate that the iodine on the 1,4-DITFB molecules undergoes a significant change in its environment upon compression. In addition, the presence of A_g and B_{3g} vibrational modes of crystalline I_2 in the released sample (near 178 and 188 cm^{-1}, respectively) suggests a gradual dissociation of iodine from 1,4-DITFB molecules, which becomes irreversible when decompressed from high pressure of 18.25 GPa. Furthermore, in the higher frequency region, the Raman peak intensity of the carbon ring breathing vibration at 1580 cm^{-1} (B_{3g}), which is affected by the C–I bond, increases with pressure up to 18.25 GPa (Fig. 4f), indicating that the polarizability of the carbon rings increases with the gradual weakening of C–I bonds[47]. The sketch maps of all the relevant vibrational modes are shown in Supplementary Fig. 6. Therefore, we propose that the iodine of 1,4-DITFB becomes more shareable with enhanced orbital coupling during the period from starting compression to the final dissociation. Such an "interstitial state" might contribute to the pressure-induced blue-shifted RTP emission.

Calculation of intermolecular interactions of 1,4-DITFB crystals

To investigate what interactions between the iodine and neighboring molecules when it is shared, we further calculated intermolecular interactions in 1,4-DITFB crystals using the independent gradient model based on Hirshfeld partition (IGMH) analysis[48] at different pressures. As shown in Fig. 5, we found that I···I interactions dominate in the 1,4-DITFB molecular crystals, followed by I···F, F···F, and I···π interactions at ambient pressure. These interactions are enhanced as pressure increases, and the enhancement of I···I interactions is most significant. The color of the isosurface representing the I···I interactions tends to change from its original green to cyan at 4.25 GPa,

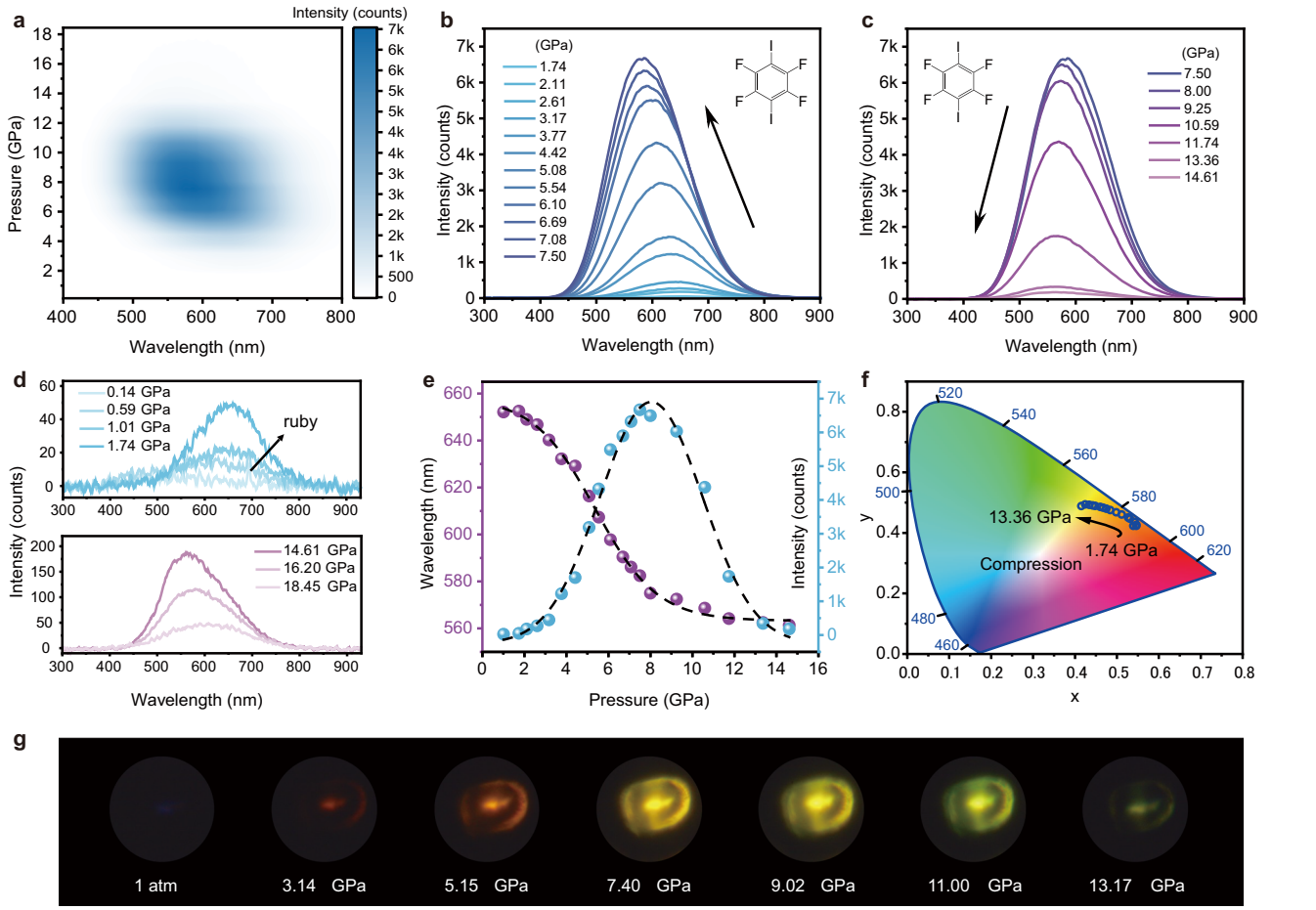

Fig. 1 | Piezochromic luminescence properties of 1,4-DITFB crystals. a 2D colormap of pressure-dependent PL intensity and wavelength. **b**–**d** In situ PL spectra of the 1,4-DITFB crystals up to 18.45 GPa. **e** Pressure-dependent PL wavelength and intensities. **f** The CIE chromaticity diagram of 1,4-DITFB crystals upon compression. **g** PL photographs of 1,4-DITFB crystals upon compression.

https://doi.org/10.1038/s41467-025-58864-6

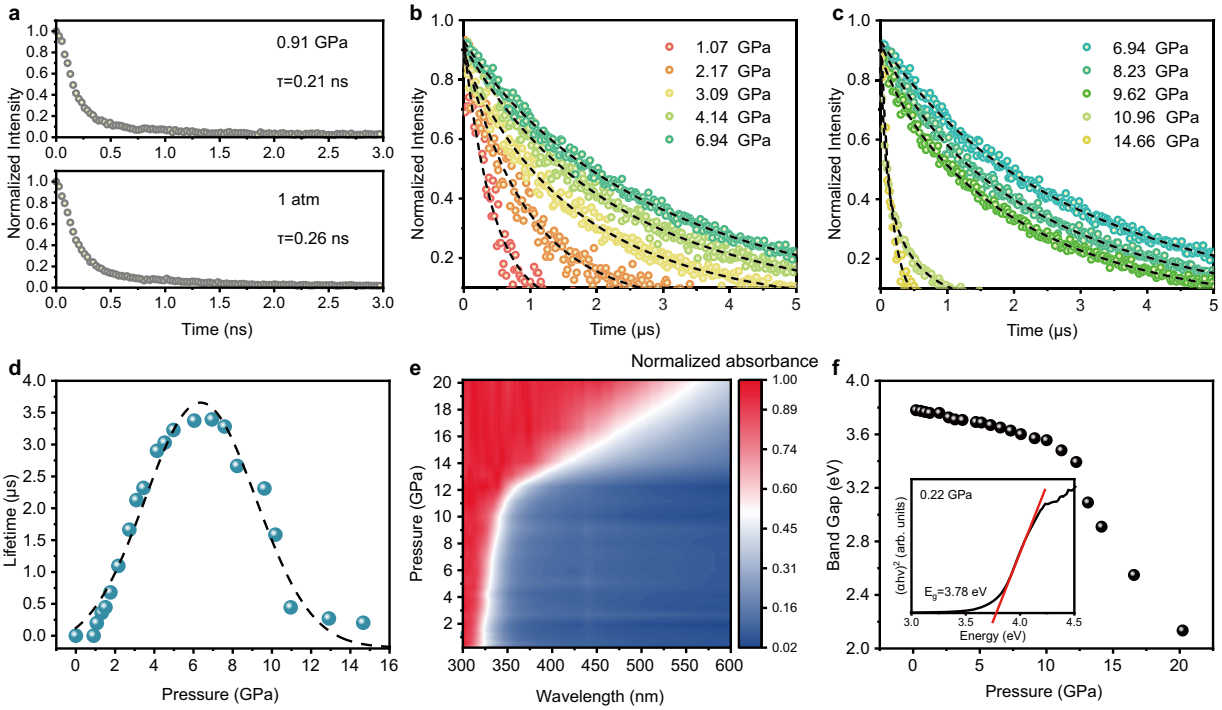

Fig. 2 | High-pressure TRPL and UV-Vis absorption measurements. a–c High-pressure TRPL spectra of 1,4-DITFB crystals. **d** Pressure-dependent PL lifetime. **e** 2D colormap of high-pressure UV-Vis absorption spectra of 1,4-DITFB crystals. **f** Variations of the optical bandgap with pressure.

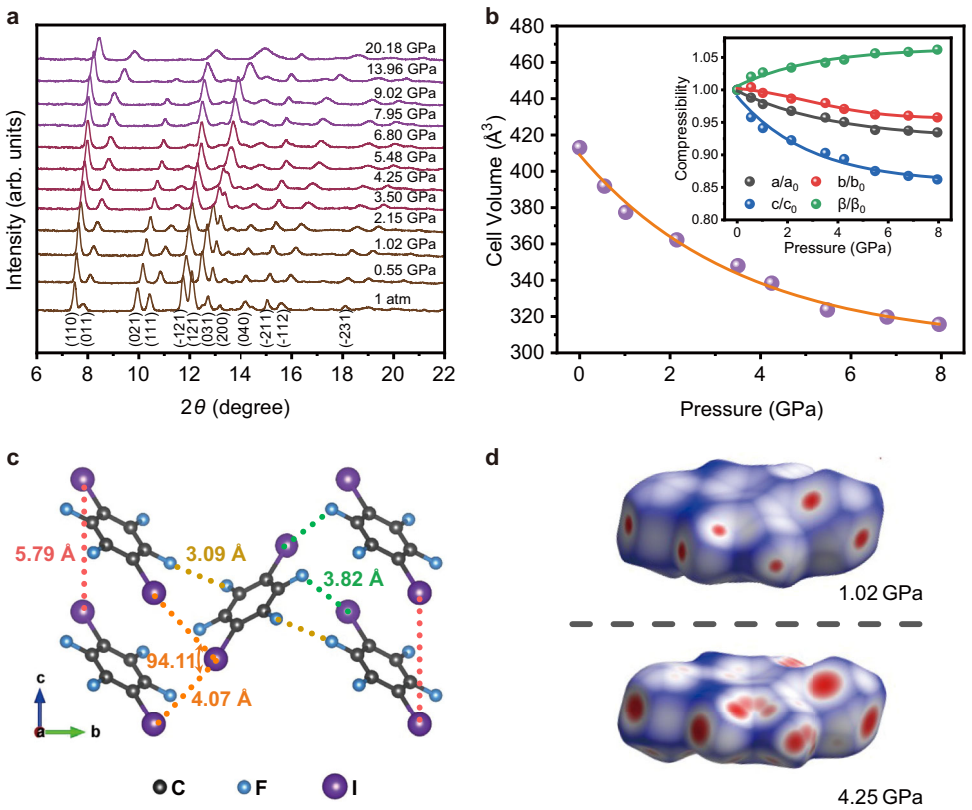

Fig. 3 | High-pressure XRD measurements and Hirshfeld surface analysis. **a** High-pressure XRD patterns of 1,4-DITFB crystals up to 20.18 GPa ($\lambda = 0.7093$ Å). **b** Plotted curves for the unit cell volume of 1,4-DITFB crystals as a function of pressure. Inset shows the compression rate of lattice constants as pressure increases, which is given by the monoclinic P21/c structure. The XRD patterns are analyzed by JADE. **c** The sketch map for molecular packing of the 1,4-DITFB crystals viewed along the *a*-axis. The distances and angles between the neighboring I···I, I···F, and F···F atoms (indicated by dashed lines) are obtained from the optimized structure at ambient conditions and measured by VESTA. **d** The Hirshfeld surface analysis of the 1,4-DITFB crystals at 1.02 GPa and 4.25 GPa.

https://doi.org/10.1038/s41467-025-58864-6

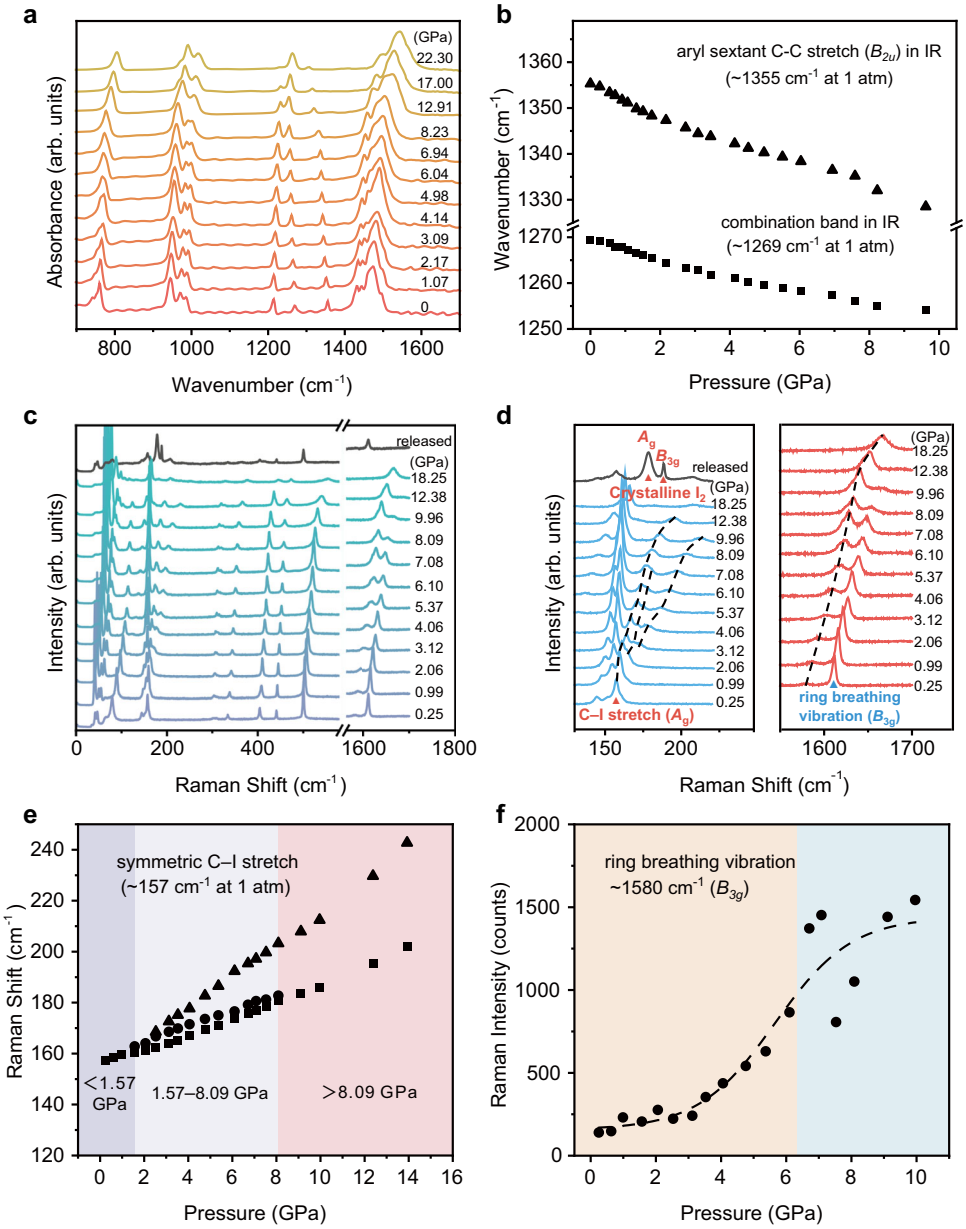

Fig. 4 | High-pressure IR and Raman spectra. a In situ IR spectra of 1,4-DITFB crystals. **b** The pressure-dependent peak positions of the observed IR modes around 1269 cm^{-1} and 1355 cm^{-1}. **c** In situ Raman spectra of 1,4-DITFB crystals. **d** The symmetric C–I stretch mode and the ring breathing vibration mode of 1,4-DITFB molecules under high pressure. **e** The pressure-dependent Raman peak positions of the symmetric C–I stretch mode. Square symbols denote the initial C–I stretch mode peak positions, while circles and triangles represent the positions of split Raman peaks emerging under high pressure. **f** The pressure-dependent Raman intensities of the ring breathing vibration mode.

indicating the I···I interactions change from the van der Waals interactions to weak attractive interactions (Supplementary Fig. 7). Note that such enhanced intermolecular interactions can explain the triple splitting of C–I stretch (A_g) under pressure (Supplementary Fig. 8). These results indicate the modification of the interactions between iodine and its surrounding atoms/molecules, as well as the enhancement of intermolecular interactions, which are crucial for the formation of the molecular aggregate necessary for the atomic orbital sharing mechanism.

Characterization of 1,4-DITFB-based cocrystals

To further verify that the anomalous pressure-induced blue-shifted RTP is related to the "shared atomic orbitals" of iodine, we employed a cocrystal strategy to hinder iodine-iodine interactions between neighboring molecules (as shown in Fig. 3c) upon compression. In this case, the diphenylacetylene (DPA) serves as molecular barrier in the synthesized DPA-(1,4-DITFB) cocrystals and breaks the "herringbone" molecular packing of 1,4-DITFB molecules that are observed in 1,4-DITFB crystals (Fig. 6a), with DPA as the donor molecule and 1,4-DITFB as the acceptor molecule[39]. XRD characterization of the cocrystals at ambient pressure (Supplementary Fig. 9) shows that the 1,4-DITFB molecules are arranged in parallel within the cocrystal and the distance between the nearest neighboring iodine atoms is relatively large (~5.42 Å), which hinders the formation of obvious halogen-halogen interactions (Supplementary Fig. 10). High-pressure XRD analyzes on the cocrystals (Fig. 6b and Supplementary Fig. 11) suggest no structural transformation upon compression. However, the high-pressure Raman spectra (Fig. 6c and Supplementary Fig. 12) are obviously different

https://doi.org/10.1038/s41467-025-58864-6

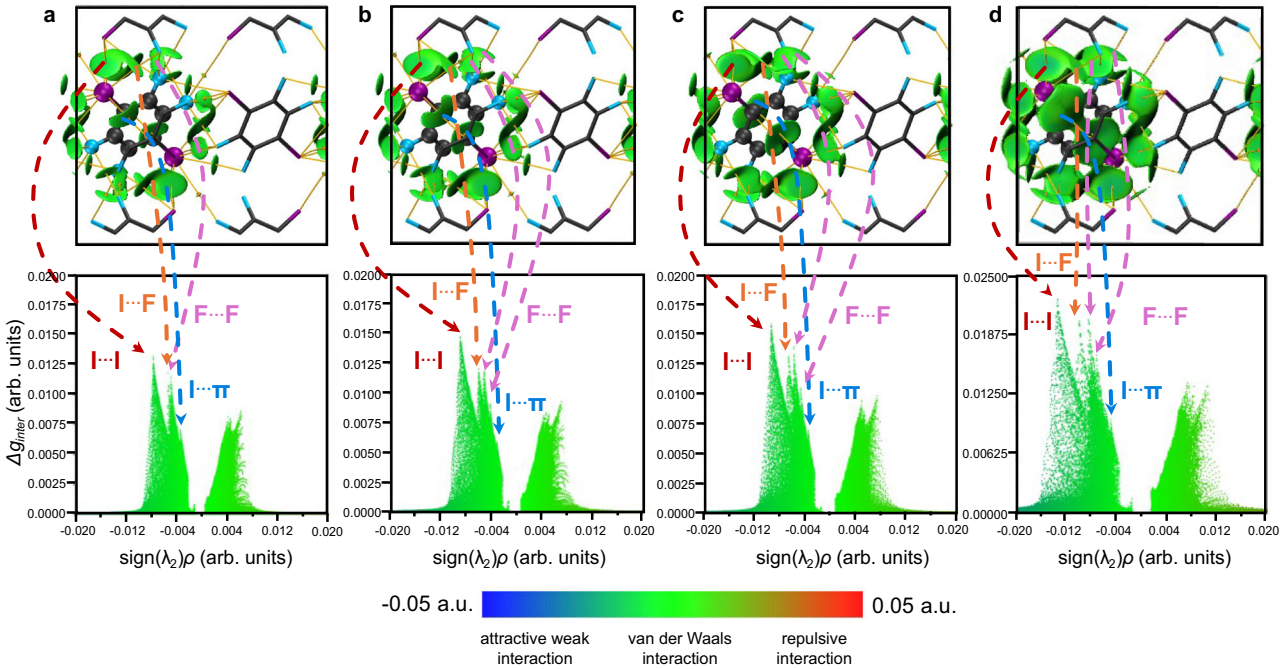

Fig. 5 | IGMH analysis of 1,4-DITFB crystals. The upper plots show crystal structures and sign(λ_2)ρ colored isosurfaces (isovalue = 0.05), and the lower plots show the scatter diagrams of the inter-fragment IGMH versus sign(λ_2)ρ of 1,4-DITFB crystals at **a** 1 atm, **b** 0.55 GPa, **c** 1.02 GPa, and **d** 4.25 GPa.

from those of 1,4-DITFB crystals, that is, no splitting in the A_g mode of C–I bonds (at 158 cm^{-1}) upon compression, suggesting no dissociation process of iodine. As a result, the cocrystals do not display any blue-shifted emission as pressure increases (Fig. 6d) and their lifetimes decrease gradually (Supplementary Fig. 13). Besides these, we observed an obvious enhanced RTP emission of cocrystals up to 2.56 GPa (Fig. 6d), which can be attributed to the inhibition of benzene ring vibrations in the 1,4-DITFB molecule, as evidenced by our IR spectra (Fig. 6e and Supplementary Fig. 14). These results further demonstrate that the unique state of iodine is responsible for the blue-shifted and enhanced emission. It is worth mentioning that the low electronegativity of iodine results in relatively weak C–I bonding[49], thus facilitating the sharing of "atomic orbitals" due to the weak binding force from C. In contrast, when iodine was replaced by bromine (Br) with higher electronegativity, only red-shifted RTP emission was observed in our comparison experiments of compressing 1,4-dibromotetrafluorobenzene (1,4-DBrTFB) crystals (Supplementary Fig. 15). Moreover, in order to better understand the roles of fluorides, we conducted high-pressure PL and TRPL measurements on 1,4-diiodobenzene (1,4-DIB) crystals (Supplementary Fig. 16). The results show that only weak fluorescence emission is present. Therefore, compared to 1,4-DIB, the F atoms introduce the I···F and F···F interactions to stabilize the SOC and emission of triplet states, resulting in a stable and anomalous RTP emission in 1,4-DITFB crystals.

Calculation of the hole-electron analysis and other luminescent properties

To gain further insights into how the sharing of "atomic orbitals" of iodine induces anomalous RTP emission upon compression, we conducted computational analysis on 1,4-DITFB crystals. In this case, the iodine atoms are suggested to affect the excited state structure of 1,4-DITFB significantly. On the one hand, the orbital sharing between neighboring iodine atoms could alter the molecular energy levels and result in blue-shifted emissions; on the other hand, the influence of the orbital overlap will enhance the radiative transition probability, contributing to enhanced RTP emission. Therefore, we optimize the structures of 1,4-DITFB crystals under pressure and analyze their excited state properties by hole-electron analysis, which can be used to describe the electronic excitation process (described as "hole→electron")[50–53]. The charge density difference (CDD) of holes/electrons from the excited state T_1 to the ground state S_0, denoted as the CDD of $T_1 \rightarrow S_0$, was calculated to analyze the phosphorescence emission process, as depicted in Fig. 7a, b. In particular, our calculations show that the lengths of the C–I bond (shown by the black dashed line) in the excited state are 2.54 Å and 2.46 Å at 1.02 GPa and 4.25 GPa, respectively, which is significantly longer than the pristine bond length of 2.08 Å at ambient pressure. In this case, iodine atoms are shared with the neighboring molecules to form cluster excitation, while the neighboring iodine provides additional holes. To further quantitatively describe the hole occupancy of iodine atoms, the excited state compositions of T_1 were calculated. The compositions of T_1 by the C-squared Population Analysis (SCPA) method[54] show that the atomic orbital contribution of the neighboring iodine increases from 1.86 % to 3.57 % when pressure increases from 1.02 GPa to 4.25 GPa. These results support the formation of an "interstitial state" of iodine in the excited state, and this state becomes more pronounced as pressure increases. In particular, the form of molecular aggregation in our calculations differs from conventional excimer excitation. In typical excimer systems[55], molecular aggregation occurs through parallel stacking stabilized by strong π–π interactions. In contrast, the formation of "shared atomic orbitals" in 1,4-DITFB does not involve such parallel arrangements or π–π interactions. Instead, it is a form of aggregation excitation dominated by I···I interactions. Meanwhile, the excitation/emission energies of 1,4-DITFB crystals in such states were calculated to demonstrate the change in energy levels. As shown in Fig. 7c, the excitation energy of the $S_0 \rightarrow S_1$ ($E(S_1)$) and emission energy of the $T_1 \rightarrow S_0$ ($E(T_1)$) changed from 4.199 eV to 4.188 eV and from 1.742 eV to 2.016 eV, respectively, as pressure increased from 1.02 GPa to 4.25 GPa, which agrees well with the experimentally observed red-shifted absorption but blue-shifted emission. Furthermore, the effect of interstitial iodine atoms on the emission intensity was investigated by calculating the overlap of hole and electron. The overlap function between the hole and electron distributions, denoted as $S_r(\mathbf{r}) = \sqrt{\rho^{hole}(\mathbf{r})\rho^{ele}(\mathbf{r})}$, in which ρ^{hole} and ρ^{ele} represent the densities of

https://doi.org/10.1038/s41467-025-58864-6

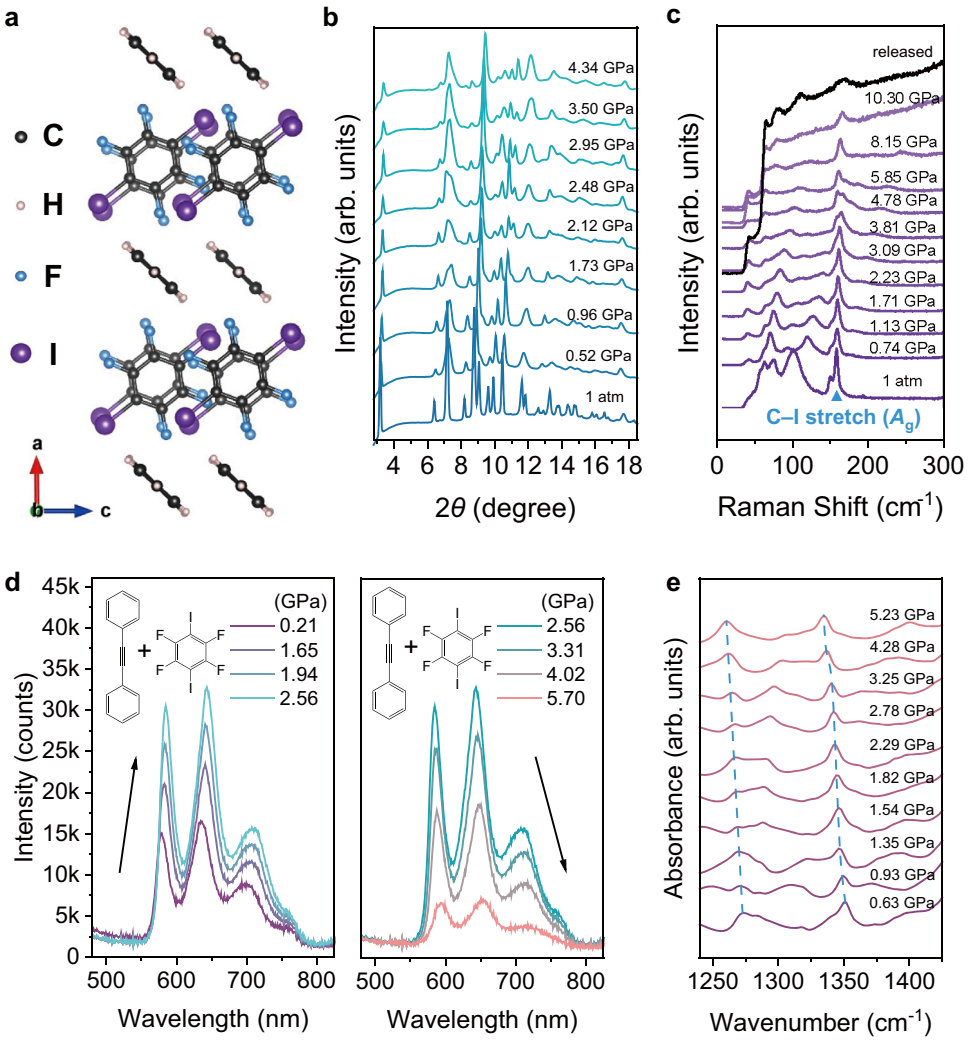

Fig. 6 | Characterization of DPA-(1,4-DITFB) cocrystals. a The sketch map for molecular packing of DPA-(1,4-DITFB) cocrystals viewed along the *b*-axis. **b** In situ synchrotron XRD spectra ($\lambda = 0.6199$ Å), **c** Raman spectra, **d** PL spectra, and **e** IR spectra of DPA-(1,4-DITFB) cocrystals upon compression. The complete high-pressure Raman and IR spectra are shown in Supplementary Figs. 12 and 14, respectively.

hole and electron[56]. The S_r values are 0.505 and 0.568 for pressures of 1.02 GPa and 4.25 GPa, respectively, indicating an increase the radiative transition probability between the T_1 state and S_0 state, thus causing an enhancement of RTP emission.

In addition, phosphorescence emission is strongly affected by ISC, and increasing the ISC rate constant (k_{ISC}) of S_1–T_1 is critical to achieving efficient RTP. Therefore, we analyzed the k_{ISC} of 1,4-DITFB crystals. According to the first-order perturbation theory and Marcus semiclassical approach in the room-temperature region, the k_{ISC} of S_1 to T_1 is expressed as Eqs. (1) and (2)[57]:

$$k_{ISC} \propto \left\langle \Psi^1 \middle| \hat{H}_{so} \middle| \Psi^3 \right\rangle / \exp\left(\Delta E_{ST}^2\right) \quad (1)$$

$$\Delta E_{ST} = E(S_1) - E(T_1) \quad (2)$$

Where $\langle \Psi^1 | \hat{H}_{so} | \Psi^3 \rangle$ is the spin-orbit coupling (SOC) matrix element between singlet and triplet states, which can be quantized using the SOC constants, where ΔE_{ST} is the first singlet and triplet splitting energy. Based on Eq. (2) and the calculated $E(S_1)$ and $E(T_1)$ discussed above, when pressure increases from 1.02 to 4.25 GPa, the ΔE_{ST} decreases from 2.457 eV to 2.172 eV, and the SOC constant of S_1–T_1 and T_1–S_0 increases from 0.24 cm^{-1} to 0.83 cm^{-1} and 3.11 cm^{-1} to 3.29 cm^{-1} (Fig. 7d), respectively. The schematic in Fig. 7e illustrates the contribution of the decreased ΔE_{ST} and the increased SOC to RTP radiation. Thus, according to Eq. 1, both the decreased ΔE_{ST} and increased SOC constants could favor the k_{ISC}, that is, the transition of electrons from singlet to triplet state is easier under pressure, leading to more efficient phosphorescence emission. All our calculations and experiments thus support the formation of "shared atomic orbitals" for iodine, which significantly affect the excitation behavior of electrons and thus contribute greatly to the anomalous piezochromic luminescence responses observed in 1,4-DITFB crystals.

Discussion

We have modulated RTP in organic materials through a strategy involving the incorporation of "atomic orbital sharing", resulting in the attainment of RTP materials exhibiting anomalous piezochromic luminescence responses. It is found that when iodine atoms exhibit characteristics of "shared atomic orbitals" and form significantly enhanced interactions with neighboring molecules in 1,4-DITFB crystals, anomalous piezochromic luminescence responses occur. The material displays an abnormally blue-shifted and enhanced RTP emission with a counterintuitively prolonged lifetime as pressure

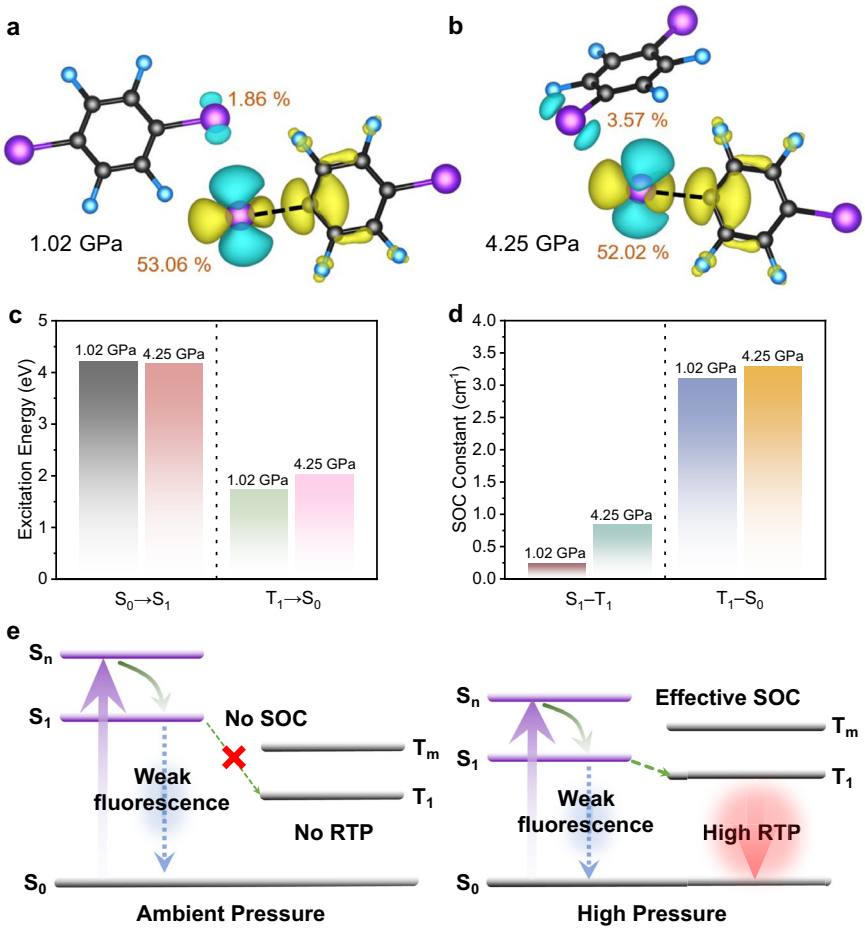

Fig. 7 | Calculated luminescent properties of 1,4-DITFB crystals. a The charge density difference (CDD) of $T_1 \rightarrow S_0$ at 1.02 GPa and **b** 4.25 GPa. The orange font represents the contribution of the iodine atom to the hole. Contributions less than 1.5% are not shown. **c** The excitation energies associated with the $S_0 \rightarrow S_1$ and $T_1 \rightarrow S_0$ transitions at 1.02 GPa and 4.25 GPa. **d** The SOC constants of S_1–T_1 and T_1–S_0 of 1,4-DITFB crystals at 1.02 GPa and 4.25 GPa. **e** Schematic illustration of the pressure-induced RTP in 1,4-DITFB crystals.

increases, which differs from the red-shifted and quenched emission observed in other organic luminescent materials reported previously. When the "atomic orbital sharing" of iodine is hindered by a co-crystallization strategy, the anomalous piezochromic luminescence responses are prohibited. By combining experiment with theory, we further reveal that such iodine state arises from strong halogen-halogen interactions, which alter the electronic structure of the excited states, leading to the blue-shifted emission, while the enhanced SOC and the inhibition of non-radiative energy dissipation contribute to the emission enhancement. This study not only provides insights into our understanding of RTP emissions in organic materials but also offers a method for designing stimuli-responsive materials for diverse applications.

Methods

Materials source, synthesis, and crystal structure

1,4-Diiodotetrafluorobenzene (1,4-DITFB, purity: 99.82%) and diphenylacetylene (DPA, purity: 99.75%) were acquired from Adamas for the experimental procedures. All chemical components were utilized in their as-received state without further purification. The DPA-(1,4-DITFB) cocrystals were prepared by solvent evaporation methods. A molar ratio of 1:2 for DPA and 1,4-DITFB was dissolved in an excessive mixture solution of chloroform and n-hexane (4:1 ratio) and ultrasonicated for 15 min. Subsequent to a 7-day solvent evaporation period under ambient conditions, the resulting transparent white flake sample of DPA-(1,4-DITFB) was obtained. The initial crystal structures of our 1,4-DITFB and DPA-(1,4-DITFB) were obtained from the Cambridge Crystallographic Data Centre (CCDC, Nos 819337 and 1060250, respectively).

High-pressure generation and in situ high-pressure experiments

High-pressure experiments were conducted using a diamond anvil cell (DAC). Samples were inserted into a 120 μm diameter hole drilled in a T301 stainless-steel gasket. Pressure calibration was achieved through the fluorescence emission of ruby within the sample chamber. Silicone oil acted as the pressure-transmitting medium (PTM) for high-pressure photoluminescence (PL), time-resolved photoluminescence (TRPL), X-ray diffraction (XRD), Raman spectroscopy, and ultraviolet-visible (UV-Vis) absorption measurements. Meanwhile, potassium bromide (KBr) acted as PTM for high-pressure infrared (IR) spectroscopy.

A home-built integrated optical measurement system was utilized for the acquisition of high-pressure photoluminescence (PL) spectra and ultraviolet-visible (UV-Vis) absorption spectra. A semiconductor UV laser (355 nm) and a deuterium-halogen lamp were used as the excitation sources to record PL and UV-Vis spectra, respectively, along with an optical fiber spectrometer (Ocean Optics, QE65 pro). The PL spectra of 1,4-DITFB and DPA-(1,4-DITFB) were collected with collection times of 1 s and 5 s, under laser powers of 1.69 mW and 23.4 μW, respectively. All the UV-Vis spectra were collected with a time of 500 ms. For high-pressure time-resolved photoluminescence (TRPL)

measurements, a pulsed laser (375 nm, Horiba DeltaDiode) with a maximum frequency of 100 MHz was employed as the excitation source, in conjunction with a Horiba Jobin-Yvon iHR320 spectrometer. High-pressure infrared measurements were carried out using a Bruker Vertex 80 V spectrometer. Raman spectra were collected using a LabRAM HR Evolution spectrometer (HORIBA Jobin-Yvon) excited by a 532 nm laser with a total power of 71.2 mW (100%) and a laser spot of ~2 μm. The Raman spectra of 1,4-DITFB and DPA-(1,4-DITFB) were recorded with collection times of 10 s and 20 s, under laser powers of 5.50 mW (10%) and 1.78 mW (3.2%), respectively. The laser power was measured with the THORLABS PM100D. For high-pressure X-ray diffraction measurements, the Rigaku Synergy Custom FR-X instrument (λ = 0.7093 Å) was utilized for 1,4-DITFB crystals, while the synchrotron radiation X-ray diffraction (λ = 0.6199 Å) was performed for DPA-(1,4-DITFB) cocrystals. All ambient-pressure powder X-ray diffraction measurements were conducted using a Bruker D8 Advance diffractometer equipped with Cu Kα radiation (λ = 1.5406 Å).

Computational details

We used the CP2K software package[52] to perform geometry optimization and electronic structure calculations, using the B3LYP/DZVP-MOLOPT-SR-GTH level with the dispersion-corrected density functional (DFT-D3(BJ)), with a grid cutoff of 500 Ry. The electronic structure properties of excited states were performed by using linear response TDDFT. The crystal structures at different pressures (1 atm, 0.55 GPa, 1.02 GPa, and 4.25 GPa) used for all calculations were obtained based on high-pressure XRD characterization. The CP2K input files and hole-electron analysis were performed by the Multiwfn program[50,51,53–55]. The Crystal-Explorer software 21.5 was employed to create Hirshfeld surface plots[58], and the IGMH analysis was plotted via VMD software[48]. The vibrational analysis and calculation of high-pressure Raman spectra were performed using the CASTEP package[59].

Reporting summary

Further information on research design is available in the Nature Portfolio Reporting Summary linked to this article.

Data availability

All data supporting the findings of this study are available within the article and the Supplementary Information Files. All other relevant data that support the findings of this study can be obtained from the corresponding authors upon request. The lattice parameters and atomic coordinates of the optimized computational models are provided in Supplementary Data 1. Source data are provided with this paper.

References

1. Zhao, W., He, Z. & Tang, B. Z. Room-temperature phosphorescence from organic aggregates. *Nat. Rev. Mater.* **5**, 869–885 (2020).
2. Kabe, R. & Adachi, C. Organic long persistent luminescence. *Nature* **550**, 384–387 (2017).
3. Hamzehpoor, E. et al. Efficient room-temperature phosphorescence of covalent organic frameworks through covalent halogen doping. *Nat. Chem.* **15**, 83–90 (2023).
4. Gu, L. et al. Colour-tunable ultra-long organic phosphorescence of a single-component molecular crystal. *Nat. Photonics* **13**, 406–411 (2019).
5. An, Z. et al. Stabilizing triplet excited states for ultralong organic phosphorescence. *Nat. Mater.* **14**, 685–690 (2015).
6. Wang, H. et al. Abnormal thermally-stimulated dynamic organic phosphorescence. *Nat. Commun.* **15**, 2134 (2024).
7. Song, J. et al. An elastic organic crystal with multilevel stimuli-responsive room temperature phosphorescence. *Matter* **6**, 2005–2018 (2023).
8. Li, H. et al. Achieving stimuli-responsive amorphous organic afterglow in single-component copolymer through self-doping. *J. Am. Chem. Soc.* **145**, 7343–7351 (2023).
9. Li, D. et al. Completely aqueous processable stimulus responsive organic room temperature phosphorescence materials with tunable afterglow color. *Nat. Commun.* **13**, 347 (2022).
10. Li, D., Yang, J., Fang, M., Tang, B. Z. & Li, Z. Stimulus-responsive room temperature phosphorescence materials with full-color tunability from pure organic amorphous polymers. *Sci. Adv.* **8**, eabl8392 (2022).
11. Nagura, K. et al. Distinct responses to mechanical grinding and hydrostatic pressure in luminescent chromism of tetrathiazolylthiophene. *J. Am. Chem. Soc.* **135**, 10322–10325 (2013).
12. Guo, S. et al. Pressure-suppressed carrier trapping leads to enhanced emission in two-dimensional perovskite $(HA)_2(GA)Pb_2I_7$. *Angew. Chem.* **132**, 17686–17692 (2020).
13. Zhao, D. et al. Harvesting cool daylight in hybrid organic–inorganic halides microtubules through the reservation of pressure-induced emission. *Adv. Mater.* **33**, 2100323 (2021).
14. Ma, Z. et al. Pressure-induced emission of cesium lead halide perovskite nanocrystals. *Nat. Commun.* **9**, 4506 (2018).
15. Hu, S. et al. Pressure-induced local excitation promotion: new route toward high-efficiency aggregate emission based on multimer excited state modulation. *J. Phys. Chem. Lett.* **13**, 1290–1299 (2022).
16. Wu, J. et al. Molecular engineering of mechanochromic materials by programmed C–H arylation: making a counterpoint in the chromism trend. *J. Am. Chem. Soc.* **138**, 12803–12812 (2016).
17. Liu, Y. et al. Piezochromic luminescence of donor–acceptor cocrystals: distinct responses to anisotropic grinding and isotropic compression. *Angew. Chem. Int. Ed.* **57**, 15670–15674 (2018).
18. Wang, J. et al. Tunable luminescence of a novel organic co-crystal based on intermolecular charge transfer under pressure. *J. Mater. Chem. C.* **6**, 8958–8965 (2018).
19. Dong, Y. et al. Piezochromic luminescence based on the molecular aggregation of 9, 10-Bis((E)-2-(pyrid-2-yl)vinyl)anthracene. *Angew. Chem. Int. Ed.* **43**, 10782–10785 (2012).
20. Zou, J. et al. Piezochromic tetracoordinate boron complex: blue-shifted and enhanced luminescence. *Angew. Chem. Int. Ed.* **61**, e202207426 (2022).
21. Zhai, C. et al. Molecular insertion regulates the donor-acceptor interactions in cocrystals for the design of piezochromic luminescent materials. *Nat. Commun.* **12**, 4084 (2021).
22. Yin, X. et al. Doping of charge-transfer molecules in cocrystals for the design of materials with novel piezo-activated luminescence. *Chem. Sci.* **14**, 1479–1484 (2023).
23. Liu, H. et al. Pressure-induced blue-shifted and enhanced emission: a cooperative effect between aggregation-induced emission and energy-transfer suppression. *J. Am. Chem. Soc.* **142**, 1153–1158 (2020).
24. Lower, S. & El-Sayed, M. The triplet state and molecular electronic processes in organic molecules. *Chem. Rev.* **66**, 199–241 (1966).
25. Baryshnikov, G., Minaev, B. & Ågren, H. Theory and calculation of the phosphorescence phenomenon. *Chem. Rev.* **117**, 6500–6537 (2017).
26. Shuai, Z. & Peng, Q. Excited states structure and processes: understanding organic light-emitting diodes at the molecular level. *Phys. Rep.* **537**, 123–156 (2014).
27. McClure, D. S. Triplet-singlet transitions in organic molecules. lifetime measurements of the triplet state. *J. Chem. Phys.* **17**, 905–913 (1949).
28. Bolton, O., Lee, K., Kim, H.-J., Lin, K. Y. & Kim, J. Activating efficient phosphorescence from purely organic materials by crystal design. *Nat. Chem.* **3**, 205–210 (2011).

29. Wang, W., Zhang, Y. & Jin, W. J. Halogen bonding in room-temperature phosphorescent materials. *Coord. Chem. Rev.* **404**, 213107 (2020).
30. Gao, Y. J., Li, C., Liu, R. & Jin, W. J. Phosphorescence of several cocrystals assembled by diiodotetrafluorobenzene and three ring angular diazaphenanthrenes via C–I···N halogen bond. *Spectrochim. Acta Part A* **173**, 792–799 (2017).
31. Gao, H. Y., Zhao, X. R., Wang, H., Pang, X. & Jin, W. J. Phosphorescent cocrystals assembled by 1,4-diiodotetrafluorobenzene and fluorene and its heterocyclic analogues based on C–I···π halogen bonding. *Cryst. Growth Des.* **12**, 4377–4387 (2012).
32. Miao, M.-s & Hoffmann, R. High-pressure electrides: the chemical nature of interstitial quasiatoms. *J. Am. Chem. Soc.* **137**, 3631–3637 (2015).
33. Lee, S. Y. et al. Ferromagnetic quasi-atomic electrons in two-dimensional electride. *Nat. Commun.* **11**, 1526 (2020).
34. Xu, T. et al. Realizing long range π-conjugation in phenanthrene and phenanthrene-based molecular crystals for anomalous piezoluminescence. *Chem. Sci.* **14**, 11629–11637 (2023).
35. Dhar, J., Karothu, D. P. & Patil, S. Herringbone to cofacial solid state packing via H-bonding in diketopyrrolopyrrole (DPP) based molecular crystals: influence on charge transport. *Chem. Commun.* **51**, 97–100 (2015).
36. Yin, G. et al. Targeting compact and ordered emitters by supramolecular dynamic interactions for high-performance organic ambient phosphorescence. *Adv. Mater.* **36**, e2311347 (2024).
37. Matsuoka, H. et al. Time-resolved electron paramagnetic resonance and theoretical investigations of metal-free room-temperature triplet emitters. *J. Am. Chem. Soc.* **139**, 12968–12975 (2017).
38. Yang, Z. et al. Pressure-induced room-temperature phosphorescence enhancement based on purely organic molecules with a folded geometry. *Chem. Sci.* **14**, 2640–2645 (2023).
39. Singh, M. et al. Recent advances of cocrystals with room temperature phosphorescence. *Adv. Opt. Mater.* **9**, 2002197 (2021).
40. Tong, S. et al. Fluorescence-based monitoring of the pressure-induced aggregation microenvironment evolution for an AIEgen under multiple excitation channels. *Nat. Commun.* **13**, 5234 (2022).
41. Xu, Z., He, Y., Shi, H. & An, Z. Room-temperature phosphorescence materials from crystalline to amorphous state. *SmartMat* **4**, e1139 (2023).
42. Spackman, M. A. & Jayatilaka, D. Hirshfeld surface analysis. *CrystEngComm* **11**, 19–32 (2009).
43. Wu, M. et al. Pressure-induced restricting intermolecular vibration of a herringbone dimer for significantly enhanced multicolor emission in rotor-free truxene crystals. *J. Phys. Chem. Lett.* **13**, 2493–2499 (2022).
44. Hanson, G. R., Jensen, P., McMurtrie, J., Rintoul, L. & Micallef, A. S. Halogen bonding between an isoindoline nitroxide and 1,4-diiodotetrafluorobenzene: new tools and tectons for self-assembling organic spin systems. *Chem. Eur. J.* **15**, 4156–4164 (2009).
45. Fu, Z., Wang, K. & Zou, B. Recent advances in organic pressure-responsive luminescent materials. *Chin. Chem. Lett.* **30**, 1883–1894 (2019).
46. Fox, M. *Optical properties of solids*. 3 (Oxford University Press, 2010).
47. Brillante, A. et al. High-pressure dissociation of crystalline para-diiodobenzene: optical experiments and car–parrinello calculations. *J. Am. Chem. Soc.* **127**, 3038–3043 (2005).
48. Lu, T. & Chen, Q. Independent gradient model based on Hirshfeld partition: a new method for visual study of interactions in chemical systems. *J. Comput. Chem.* **43**, 539–555 (2022).
49. Politzer, P., Lane, P., Concha, M. C., Ma, Y. & Murray, J. S. An overview of halogen bonding. *J. Mol. Model.* **13**, 305–311 (2007).
50. Lu, T. & Chen, F. Multiwfn: a multifunctional wavefunction analyzer. *J. Comput. Chem.* **33**, 580–592 (2012).
51. Liu, Z., Lu, T. & Chen, Q. An sp-hybridized all-carboatomic ring, cyclo[18] carbon: bonding character, electron delocalization, and aromaticity. *Carbon* **165**, 468–475 (2020).
52. Kühne, T. D. et al. CP2K: an electronic structure and molecular dynamics software package-Quickstep: Efficient and accurate electronic structure calculations. *J. Chem. Phys.* **152**, 194103 (2020).
53. Lu, T. A comprehensive electron wavefunction analysis toolbox for chemists. *Multiwfn. J. Chem. Phys.* **161**, 082503 (2024).
54. Lu, T. & Chen, F. Calculation of molecular orbital composition. *Acta Chim. Sin.* **69**, 2393 (2011).
55. Citroni, M., Bini, R., Foggi, P. & Schettino, V. Role of excited electronic states in the high-pressure amorphization of benzene. *Proc. Natl. Acad. Sci. USA.* **105**, 7658–7663 (2008).
56. Shao, Y., Lu, T., Li, M. & Lu, W. Theoretical exploration of diverse electron-deficient core and terminal groups in A–DA′D–A type non-fullerene acceptors for organic solar cells. *N. J. Chem.* **46**, 3370–3382 (2022).
57. Xiong, Y. et al. Designing efficient and ultralong pure organic room-temperature phosphorescent materials by structural isomerism. *Angew. Chem. Int. Ed.* **130**, 8129–8133 (2018).
58. Spackman, P. R. et al. CrystalExplorer: a program for Hirshfeld surface analysis, visualization and quantitative analysis of molecular crystals. *J. Appl. Cryst.* **54**, 1006–1011 (2021).
59. Clark, S. J. et al. First principles methods using CASTEP. *Z. Kristallogr. Cryst. Mater.* **220**, 567–570 (2005).

Acknowledgements

This work was supported financially by the National Natural Science Foundation of China (52225203 (M.Y.), 12274170 (M.Y.), 12304017 (C.Z.), 12104175 (J.D.)), the National Key Research and Development Program of China (2023YFA1406200 (B.L.)) and the Program of China Postdoctoral Science Foundation (2023M741351 (C.Z.)). We thank the BL15U1/BL17UM beamline and the User Experiment Assist System of the Shanghai Synchrotron Radiation Facility (SSRF) for the high-pressure synchrotron XRD measurements. We also thank the Instrument and Equipment Sharing Platform, College of Physics, Jilin University, for the ambient-pressure XRD measurements.

Author contributions

M.Y. and C.Z. conceived and supervised the study. T.X., C.Z., and Z.L. designed and performed the experiments. C.Z. carried out the theoretical study. X.Y. carried out the structure analysis. S.H., Y.S., L.Y., J.D., R.L., Q.L., and B.L. participated in the scientific discussions. T.X., M.Y., and C.Z. wrote and revised the manuscript.

Competing interests

The authors declare no competing interests.

Additional information

Supplementary information The online version contains supplementary material available at https://doi.org/10.1038/s41467-025-58864-6.

Correspondence and requests for materials should be addressed to Chunguang Zhai or Mingguang Yao.

Peer review information *Nature Communications* thanks Samuele Fanetti and the other, anonymous, reviewer(s) for their contribution to the peer review of this work. A peer review file is available.

Reprints and permissions information is available at http://www.nature.com/reprints

Publisher's note Springer Nature remains neutral with regard to jurisdictional claims in published maps and institutional affiliations.

Open Access This article is licensed under a Creative Commons Attribution-NonCommercial-NoDerivatives 4.0 International License, which permits any non-commercial use, sharing, distribution and reproduction in any medium or format, as long as you give appropriate credit to the original author(s) and the source, provide a link to the Creative Commons licence, and indicate if you modified the licensed material. You do not have permission under this licence to share adapted material derived from this article or parts of it. The images or other third party material in this article are included in the article's Creative Commons licence, unless indicated otherwise in a credit line to the material. If material is not included in the article's Creative Commons licence and your intended use is not permitted by statutory regulation or exceeds the permitted use, you will need to obtain permission directly from the copyright holder. To view a copy of this licence, visit http://creativecommons.org/licenses/by-nc-nd/4.0/.

© The Author(s) 2025